



# Fatigue crack growth in elastomers for leading edge erosion protection of wind turbine blades

Jakob Bech<sup>1,\*</sup> and Jamie Simon<sup>1,2,\*</sup>

<sup>1</sup>Department of Wind and Energy Systems, Composite Analysis and Mechanics, Technical University of Denmark, 4000 Roskilde Denmark

<sup>2</sup>LM Wind Power, Jupitervej 6 Kolding 6000, Denmark

Correspondence: Jakob Bech (jakb@dtu.dk)

**Abstract.** Fatigue crack growth has been observed as a prominent damage mode in rain erosion of wind-turbine blades, where it is driven by cyclic pulse loading from liquid-droplet impacts. This study investigates fatigue crack growth in a thermoplastic polyurethane elastomer used for leading-edge protection, linking repeated droplet impacts to controlled cyclic loading in a lab test. The plane-strain tensile double-slit test method is employed to determine the actual tearing energy during fatigue crack growth. A new analysis technique evaluates tearing energy throughout the test by tracking strain energy evolution with crack length. A novel test fixture with circular grip faces was developed to ensure efficient gripping of polymer sheets. It is examined how dwell time (the interval between sinusoidal load pulses) affects fatigue crack growth per cycle, denoted as da/dN. The material exhibits pronounced visco-elastic behavior, including cyclic stress softening. It may take several hundred cycles to stabilize with repeatable stress-strain loops, requiring a run-in period before crack growth assessment. Tests with shorter dwell times need more cycles to reach stabilization. Two dwell times are applied: 0.1 s and 1.0 s. Longer dwell times allow greater recovery between load pulses, reducing cyclic softening. When da/dN is plotted against peak strain, the cracks grow faster at longer dwell times. However, when plotted against tearing energy, the data collapses onto a single curve, indicating that tearing energy governs fatigue crack growth independently of dwell time. Measured crack growth rates span from  $0.6 \cdot 10^{-3} \, \mathrm{mm}$ to  $10 \cdot 10^{-3}$  mm per cycle, while tearing energies below a threshold of approximately  $2100 \text{ J/m}^2$  result in significantly lower growth values of  $3 \cdot 10^{-6}$  mm to  $6 \cdot 10^{-6}$  mm per cycle. This testing approach is novel for leading-edge protection materials, and crack growth resistance could become a key parameter in standards, material development, and erosion-safe turbine operation.

# 1 Introduction

Polymer-based coatings shield wind turbine blades from UV radiation, moisture and impacting particles, and provide a smooth surface, which is essential for aerodynamic efficiency. Leading edge erosion (LEE) of wind turbine blades due to impacts with rain droplets and other particles is a common failure type that causes loss of surface material (Caboni et al., 2025), roughening and degradation of aerodynamic performance (Vimalakanthan et al., 2023) and, in severe cases, exposure of the structural composite (Keegan et al., 2013; Maniaci et al., 2022). The consequences are loss of annual energy production of wind farms (Visbech et al., 2024) and costly repairs (Mishnaevsky et al., 2020). Wind turbine blade coatings are based on polymer resins with some filler materials (Mishnaevsky et al., 2020) and can be roughly categorized into hard and soft coatings. Hard coatings





are typically used as top coatings that cover the entire blades. In contrast, soft coatings are used as leading edge protection (LEP) because they are generally more energy absorbing and resilient to impact loading from rain droplets and airborne particles. The list of modern LEP systems also includes pre-molded polymer shells and tapes that are typically soft. The mode of damage and how it initiates and propagates varies for different types of leading edge protection (Maniaci et al., 2022). The durability of LEP systems is often quantified by the so-called whirling arm rain erosion test (RET), in which a rotor, the blades of which are covered by the specific LEP system, rotates at high speed in an artificially generated rain field (DNVGL-RP0171, 2018; Bech et al., 2022). The test is typically designed so that each part of the leading edge impacts identical measures of rain droplets, whereas the impact speed increases linearly with the radius. For homogeneous coatings that exhibit continuous progressive erosion behavior, the damage initiates where the impact velocity is highest after a certain quantity of impacted rain. In the regions of lower impact speed the damage initiates later. For these LEP systems rain erosion can be modeled and analyzed as a fatigue process where damage accumulates as a linear function of the amount of impacted rain and a power function of the impact velocity (Eisenberg et al., 2018; DNVGL-RP0573, 2020). Some finite element based erosion models employ a similar stress-based damage criterion assuming a homogeneous material exhibiting a progressive damage behavior (Amirzadeh et al., 2017; Doagou-Rad et al., 2020). This assumption tends to hold for classic hard and brittle coating types. Modern soft LEP materials are typically tough with visco-elastic behavior. These tend to fail in a less predictable manner, where local crack initiation and propagation dominate (Kinsley et al., 2025). Rupture in this class of LEP materials may initiate from defects or inhomogeneities and propagate as fatigue cracks (Fæster et al., 2021) as it is also the case for blade structures (Riddle et al., 2018).

#### 1.1 Stresses, strains and fracture upon impact

Upon impact between a droplet and the blade surface, transient stresses occur and propagate in microseconds. By numerical modeling local strains up to 80 percent and strain rates as high as  $10^3 \, \mathrm{s}^{-1}$  to  $10^6 \, \mathrm{s}^{-1}$  are predicted (Adler et al., 1996; Doagou-Rad et al., 2020). The actual magnitude and orientation of stresses imposed by a droplet impact depend on the impact velocity and size of the droplet and the hypervisco-elastic and acoustic properties of the surface material. Research by (Bowden et al., 1961) showed experimentally how a single impact from a high speed water jet can cause fracture. Distinct fracture patterns depended on the material properties. For a hard elastic polymer, they observed ring-shaped cracks at the surface some distance from the impact center. For rubber and other soft polymers, cracks were observed inside the bulk of the material below the impact center. For concentric repeated impacts, as in the single point impact fatigue test (SPIFT), similar crack patterns are observed (Fraisse et al., 2018; Johansen, 2020). The fatigue cracks initiate after a number of impacts, the number depending on the impact velocity. The location and orientation of the cracks are also directly linked to the stress patterns for impact on the specific materials. For hard elastic coatings, the ring-shaped cracks initiate at the surface, then propagate at each subsequent impact in a cone shape into the material. For soft hyper-visco-elastic materials, the fatigue cracks initiate inside the material beneath the impact center and progress radially in a star-shaped pattern.

For the randomly distributed droplet impacts in rain erosion, an infinitesimal material element will be exposed to transient loads at different magnitudes and orientations, (Hu et al., 2021). The position and orientation of the maximum local peak stress

https://doi.org/10.5194/wes-2025-247 Preprint. Discussion started: 28 November 2025

© Author(s) 2025. CC BY 4.0 License.



75



will change from one impact to another. In this case cracks may occur at randomly distributed inhomogeneities and defects, and the distinct crack patterns observed in single point impact fatigue may not be present. In both cases, it is a reasonable hypothesis that crack growth depends on three factors: (1) the rate and magnitude of the transient stresses and strains that are generated by the impacting droplets and controlled by the hyper visco-elastic properties of the impacted material, (2) the position, orientation, and length of existing cracks, and (3) the material's resistance to crack initiation and growth. Evans and co-authors (Evans et al., 1980) presented a fracture mechanics based model for droplet impact on an elastic substrate with a crack. They established a criterion to predict whether a crack would propagate upon an impact of a spherical projectile, depending on the radius, density and velocity of the projectile, the crack length and the elastic modulus and critical crack intensity factor of the impacted material. They defined the "damage threshold velocity" as a function of the above mentioned parameters.

#### 1.2 Time dependencies in crack growth and rain erosion testing

For soft visco-elastic materials, the stresses and strains at impact are time- and rate-dependent (Jespersen et al., 2023). This may also be the case for the parameters governing crack growth in rate dependent materials as demonstrated by (Cardwell et al., 1993).

Researchers (Hoksbergen et al., 2022) explores the Springer model for a range of materials. The Springer model does not account for rate dependent properties, however Hoksbergen notes, that for viscoelastic materials the material data going into the model must be obtained at the relevant high strain rates. Authors (Herring et al., 2021) makes the Springer analysis based on actual fatigue data. They fit the model with RET data by assuming a correlation between the strain rate and the ultimate strength of the material. Later research by (Jones et al., 2023) conclude that the viscoelastic properties obtained by a DMA test govern the rain erosion performance. Authors (Kinsley et al., 2025) perform RET at different droplet impact frequencies, while maintaining the impact speed. They describe a threshold impact frequency below which the LEP shows an elastic high cycle fatigue damage mechanism, and above which it changes to a brittle low cycle fatigue behavior.

Using a single point impact fatigue test, (Johansen, 2020) demonstrates that the number of impacts to crack initiation depends not only on the impact velocity but also decreases with decreasing time interval between impacts. This effect is partly due to hysteresis-induced heating and partly due to the time dependent recovery between subsequent impacts. Verma et al., (Verma et al., 2025), examine similar correlations applying a pulsating jet type of rain erosion test. They conclude that increased impact frequency results in fewer impacts before the end of incubation occurs. They attribute this to the material recovery effect between subsequent impacts. They also apply dry intervals where the test is paused for a period and then resumed. Dry intervals lead to increased lifetime of the coatings, as it is also described by Kinsley, (Kinsley et al., 2025) for the whirling arm RET. Time dependent recovery can be observed directly in the cyclic tensile loading of visco-elastic materials. When cyclic tension load is applied with a constant amplitude of elongation and the material is not allowed enough time to recover fully between each load cycle, the material gradually loses stiffness, and the load-displacement loop converges after a number of cycles. The work of deformation is then reduced from the initial cycle to the state where the loops stabilize (Bai et al., 2020). This, known as the Mullins effect or stress softening, can be either reversible or irreversible. Harbour et al., (Harbour et al.,



100

120



2007) examined the effect of pauses for rubber in a plane strain fatigue crack growth test. They applied sequences of loading pulses, with fixed strain amplitudes, separated by pauses, dwell times, and observed that the crack growth rates increased for increased dwell times. It may seem contradictory that increased dwell time leads to longer life in RET, (Kinsley et al., 2025; Verma et al., 2025), whereas it causes increased crack growth rates in fracture mechanics testing (Harbour et al., 2007). However, this is likely because the droplet impact test is load or energy driven because the impact energy in each subsequent droplet is constant, whereas the fatigue crack growth test is displacement controlled and consequently stress softening causes the stiffness, peak load and strain energy to decrease with increasing cycle number. Dwell times allow the material to recover, and the next load sequence will resume at a higher stiffness compared to the later cycles of the previous sequence. In fatigue crack growth testing, the time interval between individual load pulses, the dwell period, can also affect the crack growth rate (Ghosh et al., 2014).

# 1.3 Fatigue crack growth characterization

The crack growth behavior of materials is studied in the field of fracture mechanics, which correlates crack growth with material properties and loading conditions. The critical energy release rate  $G_c$  is a material property that determines the energy per area required to propagate a crack. The energy release rate G for an elastically loaded specimen with a crack can be equated with the potential strain energy that is released when the crack propagates. The corresponding property for crack growth on thin sheets made of, e.g., rubber materials is often denoted tearing energy T (Rivlin et al., 1953). The pure shear tensile test, also called the plane strain test, with one or two slits is often used for crack growth testing. The specimen is wide and has a short distance between the grips. Hence the material is constrained from contraction in the width direction. The cracks can grow in steady state because the test specimen, when correctly proportioned, has a stress free section behind the crack tips and a section of uniform plane strain ahead of the crack tips. From an energy balance analysis (Rivlin et al., 1953) shows that the tearing energy is given by

$$T = wh_0 \tag{1}$$

By a J-integral analysis (Rice, 1968) also arrives at  $J = wh_0$  where w is the strain energy density in the plane strain section and  $h_0$  is the length of the specimen (distance between grips) in the non-strained condition. T is also used as the load parameter in the plane strain fatigue crack growth test (Gent et al., 1964), where for rubber there is a fatigue limit of T below which the crack growth is negligible (Lake et al., 1965). Authors (Cardwell et al., 1993) demonstrate that the strain energy function depends on the loading rate and correlates with the visco-elastic properties.

Thus, there are two essential parameters to determine throughout a fatigue crack growth (FCG) test using the plane strain test setup. One is the cracks length versus number of cycles. The other is the actual tearing energy imposed during growth of the fatigue cracks. For the latter the strain energy density in the plane strain zone must be determined. Different approaches are used to measure and calculate the actual strain energy density and tearing energy imposed on the crack during FCG testing. Studies by (Stadlbauer et al., 2013), using a single-edge notch specimen tension test setup, employed the positive part of the



135



area under the force-deflection (FD) curve, the uncracked ligament length and initial height in the determination of the tearing energy. Works by (Ghosh et al., 2014), determined the crack-growth-rate vs. tearing energy curve using a strain energy density function constructed from a loading response of an uncracked specimen.

For the plane strain tensile test the grips need to be wide to ensure the plane strain constraint. Rubber-like materials are difficult to grip because of their softness and the large strains often applied. When using traditional tensile grips with plane jaw faces the material tends to slip when a tensile strain is applied, because the material contracts in the thickness direction in and near the gauge section. Molded test specimens with beads and specially designed grips are used in some laboratories (Ghosh et al., 2014). However it is often desirable to test specimens cut from sheet material. For this purpose a varying grip pressure can be a solution. Researchers (Kocjan et al., 2023) presented a grip design clamping a sheet between a knurled cylinder and a semicircular part allowing a varying compression ratio along the grip section.

A material's resistance against rain erosion can be characterized by its ability to resist damage initiation and progression, and by the rate at which damage propagates once it has initiated (Pugh et al., 2021). Several authors suggest that the rain erosion performance of LEP materials may be correlated with fracture toughness and crack sensitivity (Evans et al., 1980; Keegan et al., 2013; Pugh et al., 2021). In design, testing and analysis of wind turbine blade structures, fracture mechanics has become a well established field of research (Amirafshari et al., 2021; Ji et al., 2014). Fracture mechanics testing and analysis is also applied to cyclically loaded elastomer materials such as compounds for tires and drive belts (Sundararman et al., 2009; Ghosh et al., 2014). However, fracture mechanics based analysis and mechanical characterization of leading edge protection for wind turbine blades has not been found in literature by the present authors. The present paper proposes to introduce fracture mechanics as a novel direction in the analysis and mechanical characterization of leading edge protection materials and systems for wind turbine blades.

https://doi.org/10.5194/wes-2025-247

Preprint. Discussion started: 28 November 2025

© Author(s) 2025. CC BY 4.0 License.





#### 1.4 Problem statement

Recent literature shows that fatigue crack growth is an important damage mode in leading-edge erosion on wind turbine blades. Several testimonies from partners in the IEA Wind Task 46 and at the annual International Symposium on Leading Edge Erosion indicate that localized cracking, compared to progressive erosion, is becoming an increasingly dominant mode of damage for modern LEP systems. This is also the case for the LEP system examined in the present paper. Rain-erosion testing and subsequent X-ray computed tomography analysis of the eroded sample revealed locally occurring cracks surrounded by virtually undamaged material, see Figure 1.

Although fracture mechanics concepts such as the critical tearing energy threshold for negligible crack growth are well established for a range of elastomeric materials, corresponding knowledge for leading-edge protection (LEP) systems remains limited. In particular, the influence of loading conditions representative of liquid droplet impact (such as loading rate, dwell period and load amplitude) on the tearing energy threshold governing fatigue crack growth in modern LEP materials has not been investigated.

160 The study, therefore, investigates the effect of dwell time, load amplitude, and tearing energy on the crack growth rate in a polyurethane-based LEP material containing pre-existing cracks, using a fracture mechanics tests.

The paper is structured with a methods section 2, introducing a novel method for determining the tearing energy T in fatigue crack growth testing, and describing the experimental test setup, design considerations and data analysis. Section 3 contains the results and related observations and discussion. Section 4 presents the conclusions, perspectives and ssuggestions for future work. Appendix A1 provides a list of abbreviations and general nomenclature. It also includes two tables that will be referenced throughout the paper.







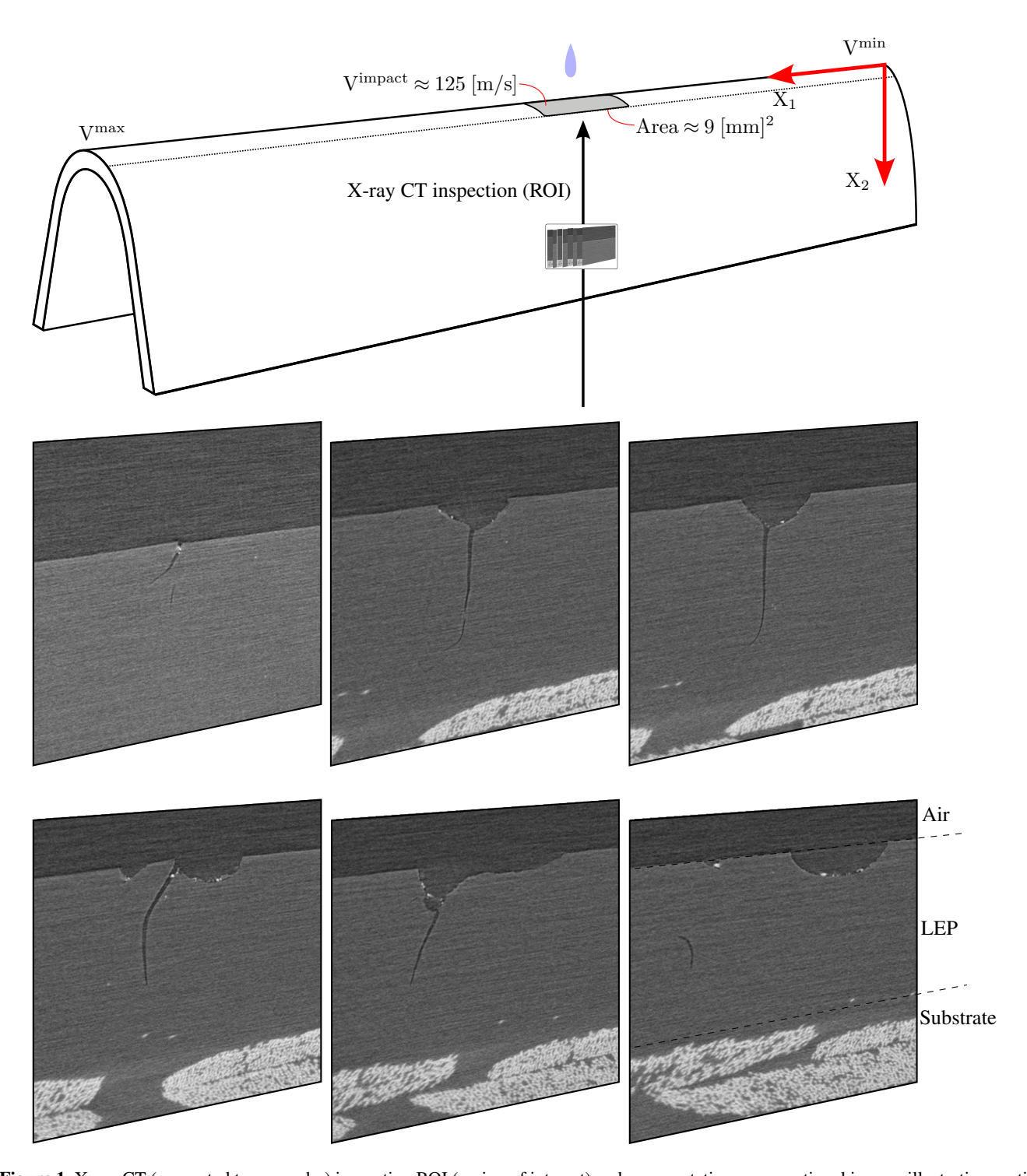


**Figure 1.** X-ray CT (computed tomography) inspection ROI (region of interest) and representative cross-sectional images illustrating spatial crack patterns after RET exposure in a laboratory-scale sample. Please note that the RET-sample is not to scale.





#### 2 Method for testing and analyzing fatigue crack growth in elastomer sheet

The experiments of the present paper were designed to characterize the cyclic crack growth behavior of an elastomeric polyurethane sheet. A new fixture with semi-circular grip faces was developed to ensure efficient gripping of the elastomer sheet. To account for the loading conditions of rain impact, a pulse loading scheme is applied, where a short pulse is followed by a dwell time before the next loading pulse.

#### 2.1 Determining the tearing energy in fatigue crack growth testing

The plane strain test with two slits, also known as the pure shear test, was chosen for fatigue crack growth (FCG) testing because it emulates steady-state crack growth and simplifies the analysis due to a plane strain zone between the crack tips (Rivlin et al., 1953). A two slit configuration was chosen because it gives symmetric loading on the fixture and load cell and twice the amount of crack growth data, da/dN, per test. Please consider the setup in Figure 2. A thin sheet is clamped at the upper and lower edges, where it is constrained from deformation in the horizontal- or 1-direction. The dimensions in the unloaded condition are width  $l_0$ , length  $h_0$  and thickness  $b_0$ . At the free edges it has slits or pre-cracks of length  $a_1$  and  $a_2$ .

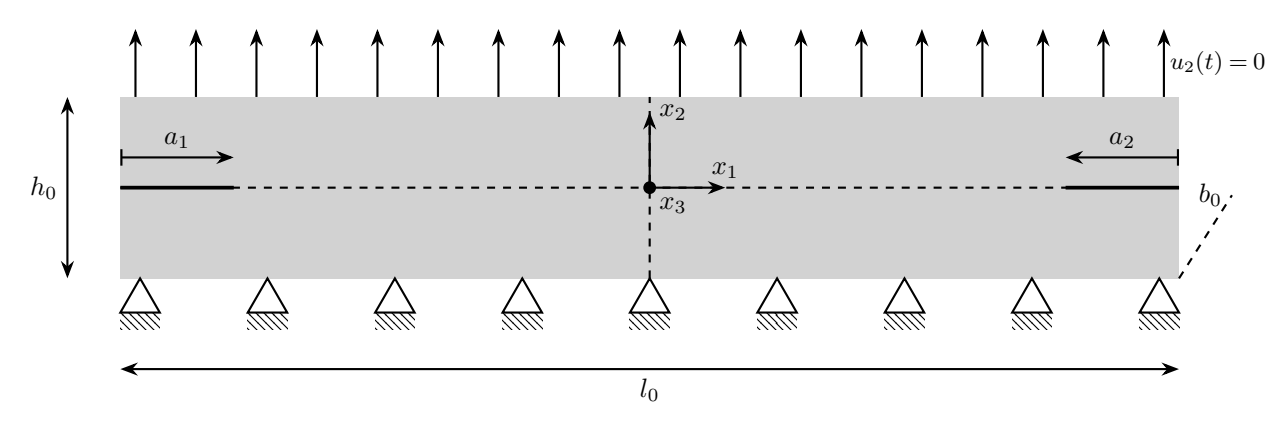


Figure 2. Schematic of the plane strain double slit tension setup for a thin plate/sheet with  $l_0$ ,  $h_0$  and  $b_0$  representing the initial width, height and thickness, respectively. The crack lengths are denoted  $a_1$  and  $a_2$ .

In this work the tearing energy will be determined by comparing two stages of the FCG test at cycle N and cycle  $N + \Delta N$ . In each cycle the test specimen is exposed to a uniform displacement  $u_2(t)$  along the  $x_1$ ,  $x_3$  plane at  $h_0/2$ , see Figure 3. Three zones, A, B an C of different deformation states can be identified. The following assumptions apply to the analysis: 1) The cracks are sufficiently long to leave zone A stress free. 2) The distance between the two crack tips is long enough to have a zone C which is unaffected by the strain field near the crack tips. 3) The aspect ratio  $L_c/h_0$  of zone C is high enough to ensure a uniform plane strain condition in zone C with zero strain in the  $x_1$ -direction. 4) Each load cycle applies the same elongation  $u_2$  to the specimen, and the hysteresis behavior (cyclic stress-strain behavior) is independent of the number of load cycles throughout the analysis.





The strain energy, w, of the plane strain zone will be determined by comparing two stages of the FCG test at cycle N and cycle  $N+\Delta N$  between which the two cracks grow by  $\Delta a_1$  and  $\Delta a_2$  and consequently the width of zone C of plane strain is reduced from  $L_{\rm C}$  to  $L_{\rm C}-(\Delta a_1+\Delta a_2)$  as illustrated in Figure 3.

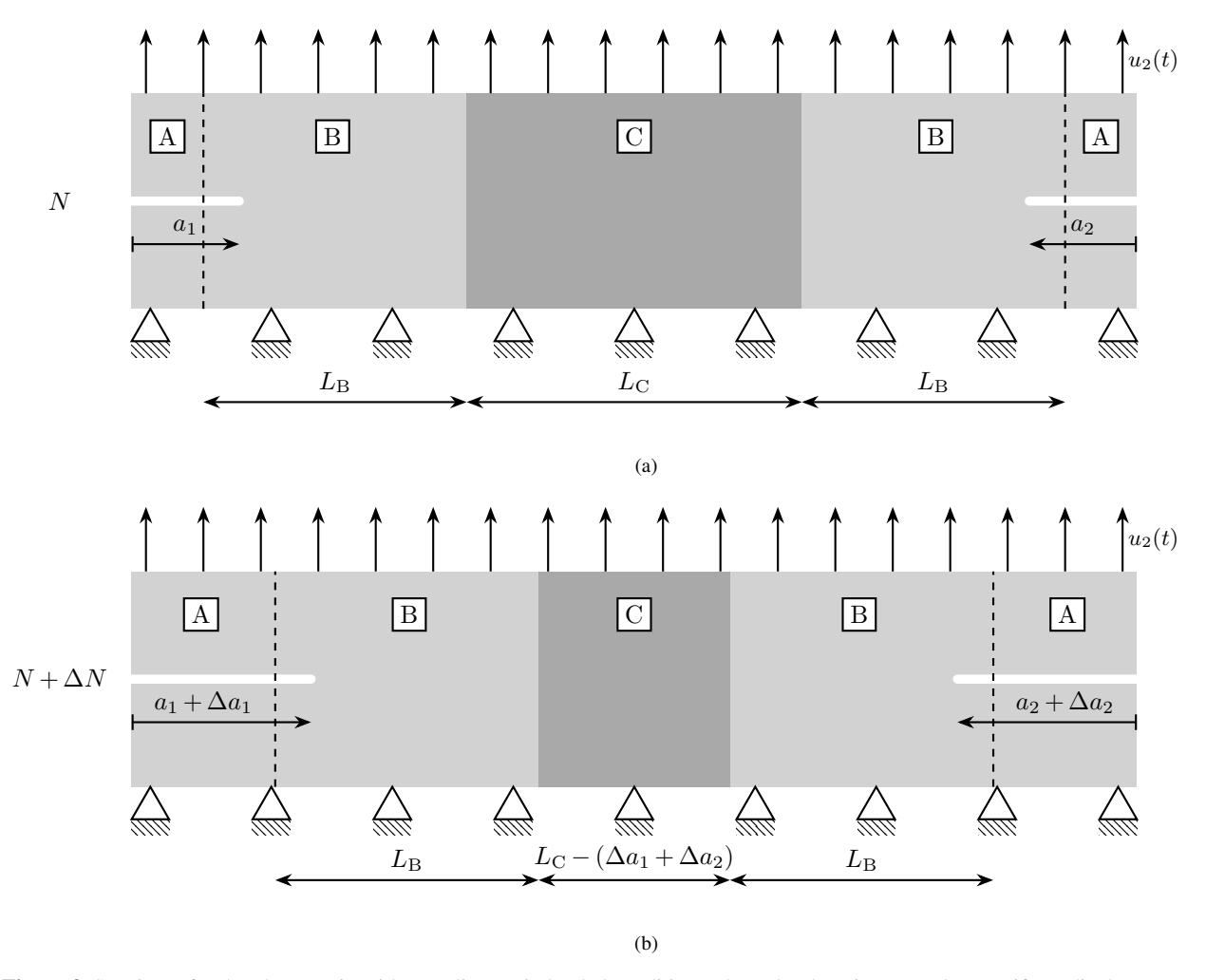


Figure 3. Specimen for the plane strain with two slits test in loaded condition, where the sheet is exposed to a uniform displacement  $u_2$  along the  $x_1, x_3$  plane at  $h_0/2$ . (a) at cycle N with crack lengths  $a_1$  and  $a_2$  and (b) cycle  $N + \Delta N$  with crack lengths  $a_1 + \Delta a_1$  and  $a_2 + \Delta a_2$ .

As the cracks progress with increasing cycles the remaining section between the crack tips is reduced, and so is the load, and work, required to stretch the reduced specimen. Because zone A is stress-free, and zone B, which includes the complicated stress fields at the crack tip, is identical at both stages, the change in work of deformation from cycle N to cycle  $N + \Delta N$  corresponds to the contribution of the part of zone C of width  $(\Delta a_1 + \Delta a_2)$  that is present in cycle N and has been removed at cycle  $N + \Delta N$ .

The deformation work of the removed part of zone C is given by  $\Delta W = W_N - W_{N+\Delta N}$ , as depicted in Figure 4.





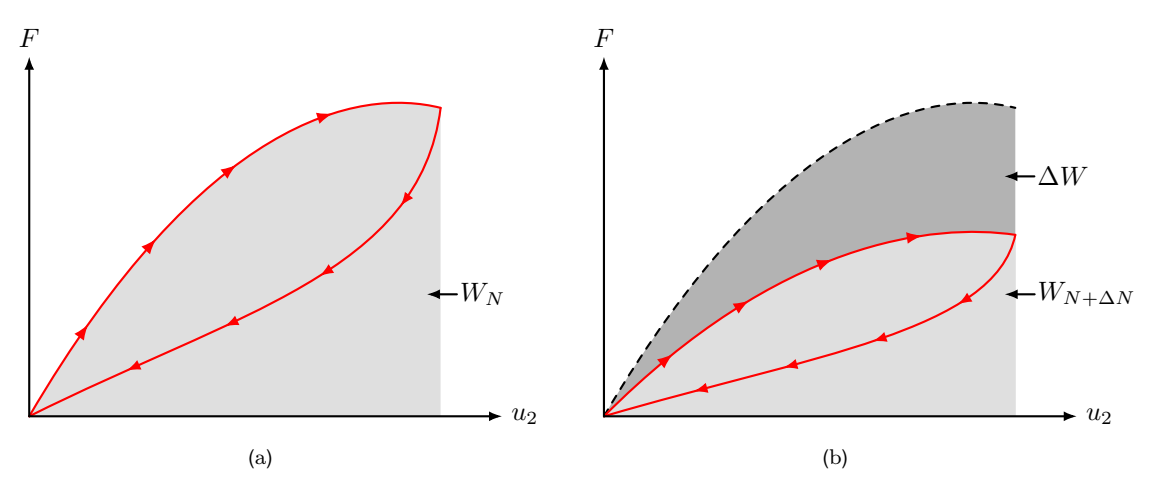


Figure 4. Load-displacement curves illustrating the work of loading that is (a)  $W_N$  for cycle N with distance between crack tips L and (b)  $W_{N+\Delta N}$  for cycle  $N+\Delta N$  with distance between crack tips  $L-\Delta L$ .

At N cycles the work of strain is

$$W_N = W_{C,N} + W_B \tag{2}$$

The contribution from zone C is

$$200 W_{C,N} = wL_C b_0 h_0 (3)$$

where w is the strain energy density in zone C. While  $W_B$  remains constant, at  $N+\Delta N$  cycles the contribution of deformation work in zone C is reduced to  $W_{C,N+\Delta N}=w(L_C-(\Delta a_1+\Delta a_2))b_0h_0$ . The difference in strain energy  $\Delta W=W_N-W_{C,N+\Delta N}$  from cycle N to cycle  $N+\Delta N$  can now be written

$$\Delta W = w(\Delta a_1 + \Delta a_2)bh_0 \tag{4}$$

205 isolating w and inserting it in Equation 1 yields

$$T = \frac{1}{b_0} \frac{\Delta W}{\Delta (a_1 + a_2)} \tag{5}$$

Equation 5 will be used to determine T in the FCG test.

# 2.2 Experimental test setup, design considerations & sample preparation

The test fixture designed for the present study adapts to the concept of partially circular grip faces as illustrated in Figure 5. The inner grip face is 90 degrees of a cylinder with radius  $r_i = 10 \,\mathrm{mm}$ . Its right counterpart has a slightly larger radius,  $r_o$ , leaving space for the test material between the two. The grip pressure at 90 degrees is determined by the tension of the bolts, whereas at 0 degrees the specimen is restricted by the fixture geometry and compressed to fit in the gap  $r_o - r_i$ , which is approximately two thirds of the specimen thickness.





The fixture was mounted in an Instron E3000 Electro-pulse test machine. The test specimens were cut into rectangular shapes of 80x46 mm. Precuts of 15 mm in length were cut with a doctor's blade. The specimens were clamped in the test fixture shown in Figure 5. The fixture design enables a gripping zone of 80 mm width, and the gripping mechanism maintains gripping even at high strains and substantial contraction in the thickness direction. The specimens were clamped in the full width. The initial free length between the grips was 10 mm.

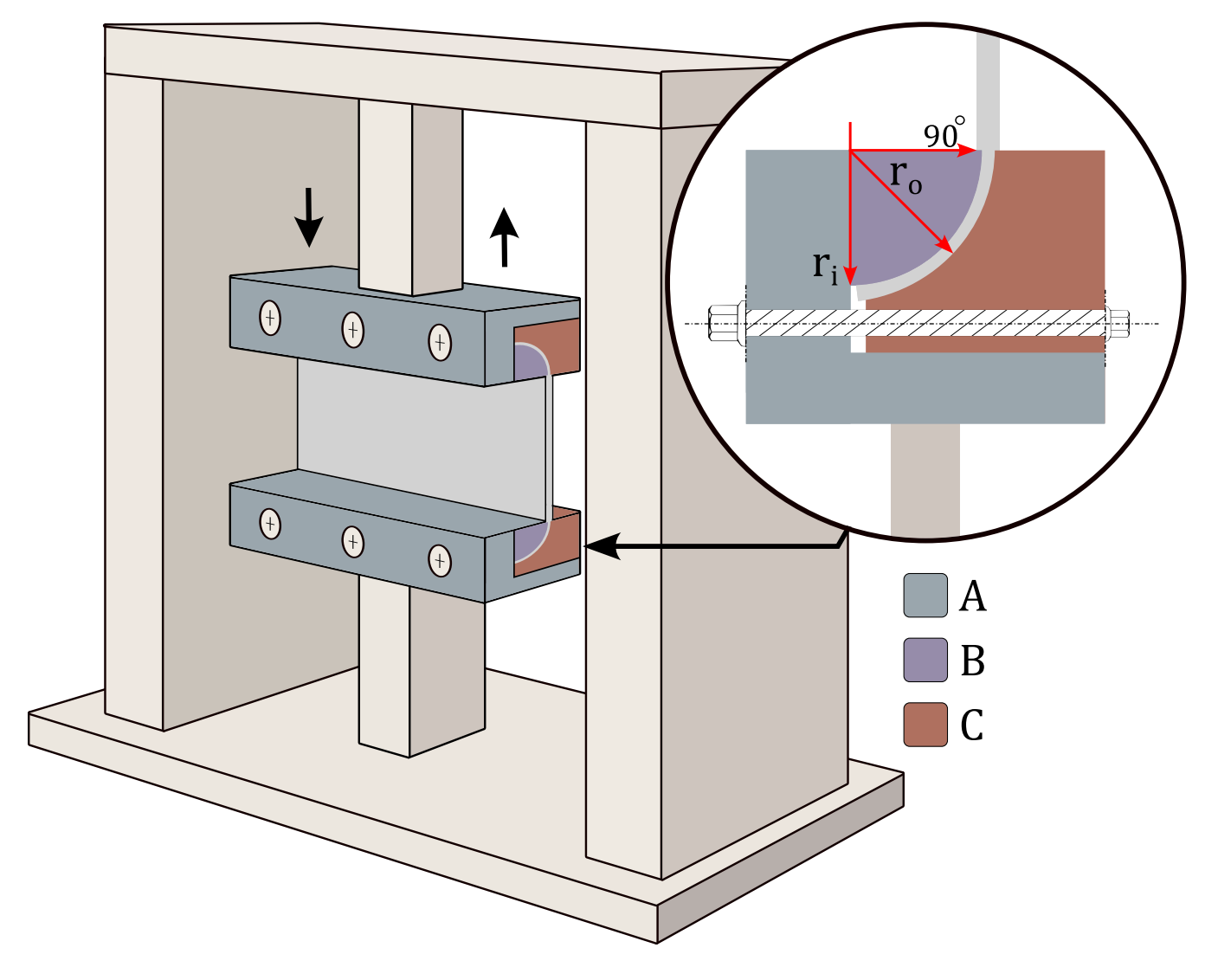


**Figure 5.** Graphical and conceptual representation of test setup on an un-notched specimen using the developed grip design. With A, B, and C constituting the different parts of the gripping mechanism.



220

230



#### 2.3 Specific impact frequency & loading conditions

In rain erosion the specific impact frequency (ASTM G73)  $f_i = (a/b)\Psi V$  is a factor indicating the frequency of impacts per projected area a of an impacting liquid body of volume b. In a rain field with evenly distributed spherical droplets of diameter d the specific impact frequency  $f_i$  is calculated by Equation 6.

$$f_i = \left(\frac{3}{2d}\right) \Psi V_{\text{impact}} \tag{6}$$

where  $V_{\rm impact}$  is the impact of the droplet relative to the exposed body. The volume concentration of liquid in a rain field,  $\Psi$ , is obtained from the rainfall rate,  $\dot{I}$ , and the terminal falling velocity of the droplet,  $V_{\rm droplet}$ , as such

$$\Psi = \frac{\dot{I}}{V_{\text{droplet}}} \tag{7}$$

In the crack growth test the period between subsequent droplet impacts is simulated by applying a dwell time,  $t_d$ , between load pulses. The dwell time was chosen based on impact frequencies computed from data using the findings from (Bech et al., 2018, 2022) (Please see Table A2 & Table A3). Although, the characteristic impact period is within the range of 1.0 and 100 seconds, the dwell-times employed in this study are 0.1 and 1.0 seconds. The parameters were chosen due to time-constraints and observable differences in stable-hysteresis loops.

The displacement control module utilizes a time-dependent sinusoidal displacement profile to simulate the transient impact response between a wind turbine blade and a single water droplet. The waveform is characterized by a pulse time,  $t_p$ , and a dwell time  $t_d$ . The minimum-to-maximum displacement ratio is set to zero to replicate a scenario in which the transient stress response from a single droplet impact has fully decayed before the next impact occurs, controlled through  $\phi$ , representing the load-active values of time during the fatigue process.





The displacement profile is given in Equation 8 and depicted in Figure 6

$$u_2(t) = \begin{cases} \frac{u_2^{\text{max}}}{2} \left[ 1 + \sin\left(2\pi\phi - \frac{\pi}{2}\right) \right], & 0 \le \phi \le 1\\ 0, & \text{otherwise} \end{cases}$$
 (8)

$$\phi = \operatorname{mod}(t, t_d + t_p)/t_p$$

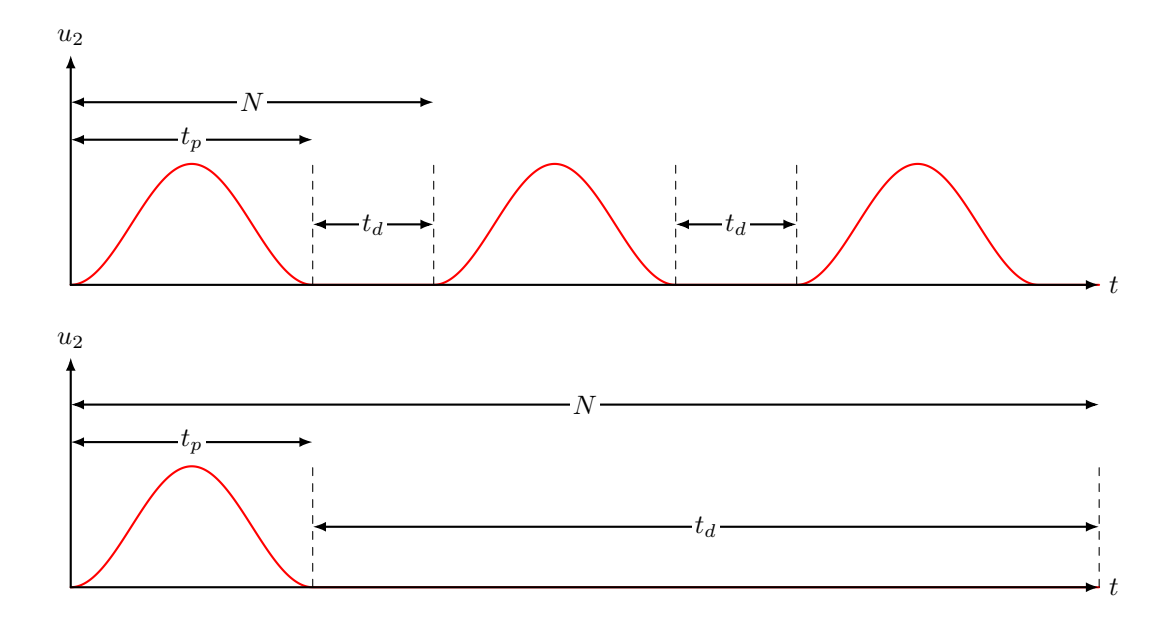


Figure 6. Illustrating the cyclic disposition during fatigue loading, programmed into the load control software. The module utilizes a displacement control setting with a load and unload profile described by a sinus function. The parameters  $t_d$  and  $t_p$  are short for dwell/hold and puls times, respectively, with N representing a full cycle period.

When the pulse displacement is applied, after a running-in period, the two cracks typically grow at approximately constant and similar rates. During the test, data of load and position peak values as well as full hysteresis loops are collected at regular intervals. In parallel a digital camera is configured to capture an image of the specimen at the peak displacement and crack opening at set intervals. The test continues until a minimum peak load criterion is reached, typically when the remaining section between the crack tips is reduced to approximately 10-20 mm.





255

# 2.4 Analysis of crack growth experiment

The work of deformation, W, that goes into the system during a single cycle is computed as the integral of the load over the displacement curve from minimum to maximum elongation, for each cycle during the FCG experiment. The crack lengths,  $a_1$  and  $a_2$ , are determined by measuring the change in pixels from cycle N to  $N + \Delta N$ , followed by conversion using the pixel to mm ratio. The work and crack distances are plotted against the number of cycles, as illustrated in Figure 7a and b. Domain II constitutes the analysis region of interest. This interval is reached when the cracks grow at approximately similar rates,  $da_1/dN \approx da_2/dN$ , and the material has reached stable values in terms of W. The crack growth rates and tearing energy are determined from the slope in domain II, as seen in Figure 7b and c.

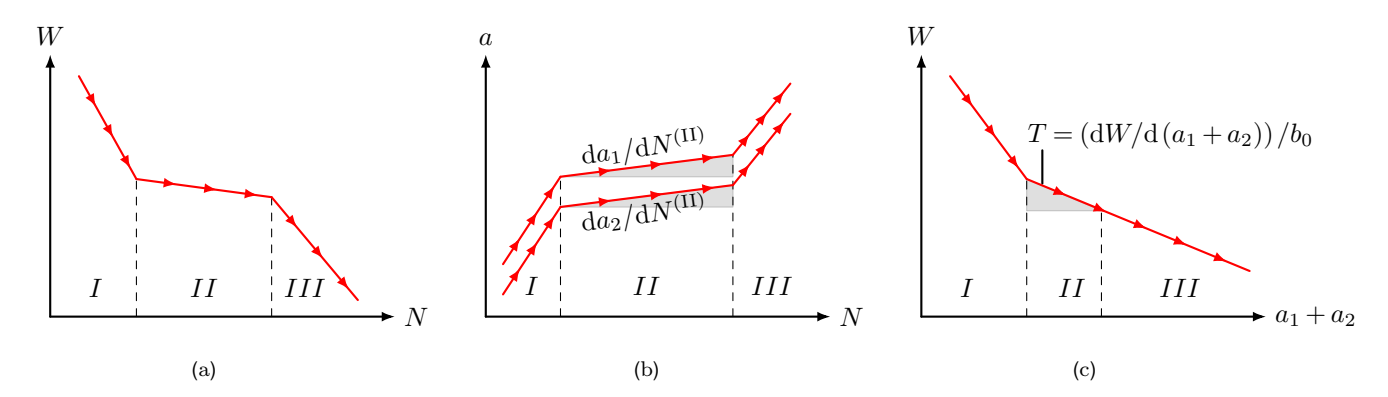


Figure 7. Illustrating the determination process for evaluating crack growth rate and tearing energy. (a) Work of deformation, W, and (b) crack lengths,  $a_1$   $a_2$ , plotted versus cycle number, N. (c) The tearing energy, T, is determined from the slope in domain II. Domain II constitutes the region where the two cracks grow at approximately equal rates,  $da_1/dN \approx da_2/dN$ , and where W is not affected by stress-softening.



270

275



#### 3 Results & discussion

#### 3.1 The effect of dwell period in cyclic loading

Figure 8 & 9 show, respectively, the load–displacement curves for an uncracked specimen, illustrating the initial and cycle 2000 hysteresis loops, and the corresponding peak loads as a function of cycle number for different dwell times.

For a dwell time of 0.1 s the peak load and work reduces from approximately 221 N and 0.28 J in cycle 1 to 126 N and 0.15 J in cycle 2000, Figure 8a. After the test, the material is left to recover for 10 minutes. Then, a new test sequence is done with a dwell time of 1 s. In the first cycle the material has almost recovered to it initial state with a peak load and work of 215 N and 0.27 J, followed by a reduction at cycle 2000 of 171 N and 0.22 J, Figure 8b. The material is left to recover for an additional 10 minutes and the test is repeated with a dwell time of 10 s. Again, the material almost recovers to its original state with a measured peak load and work of 218N and 0.28 J, followed by a reduction at cycle 2000 of 211 N and 0.27 J, Figure 8c. Here, the material almost fully recovers between the cycles.

The number of cycles required for peak load stabilization decreases with increasing dwell time, indicating that the material's load-carrying capacity (energy uptake) is significantly reduced when insufficient time is allowed for relaxation to happen between successive load cycles, Figure 9 (a) and (b). Additionally, the gradient of the load–unload curve from the initial to stabilization phase undergoes a notable change for  $t_d = 0.1$ , but not for  $t_d = 10$  s. Moreover, the ability to restore load-carrying capacity and curve shape suggests reversible molecular changes within the rubbery phase of the elastomeric system, attributed to the Mullins effect (Harwood et al., 1965), commonly referred to as stress softening. Most notably, the Mullins effect depends on the dwell time (i.e., the time between two cycles). When the dwell time is reduced to 1 s or 0.1 s, both stiffness and energy density decrease. This dependence shows that the stress-softening response, stiffness, and energy density require a run-in period before reaching stable values/conditions as seen in Figure 9 (a) and (b). The Electro-pulse test machine was unable to maintain a constant load amplitude as the specimen stiffness decreased. This is the reason why load cycles with low stiffness result in higher peak displacement as seen in Figure 8 (a) and (b).







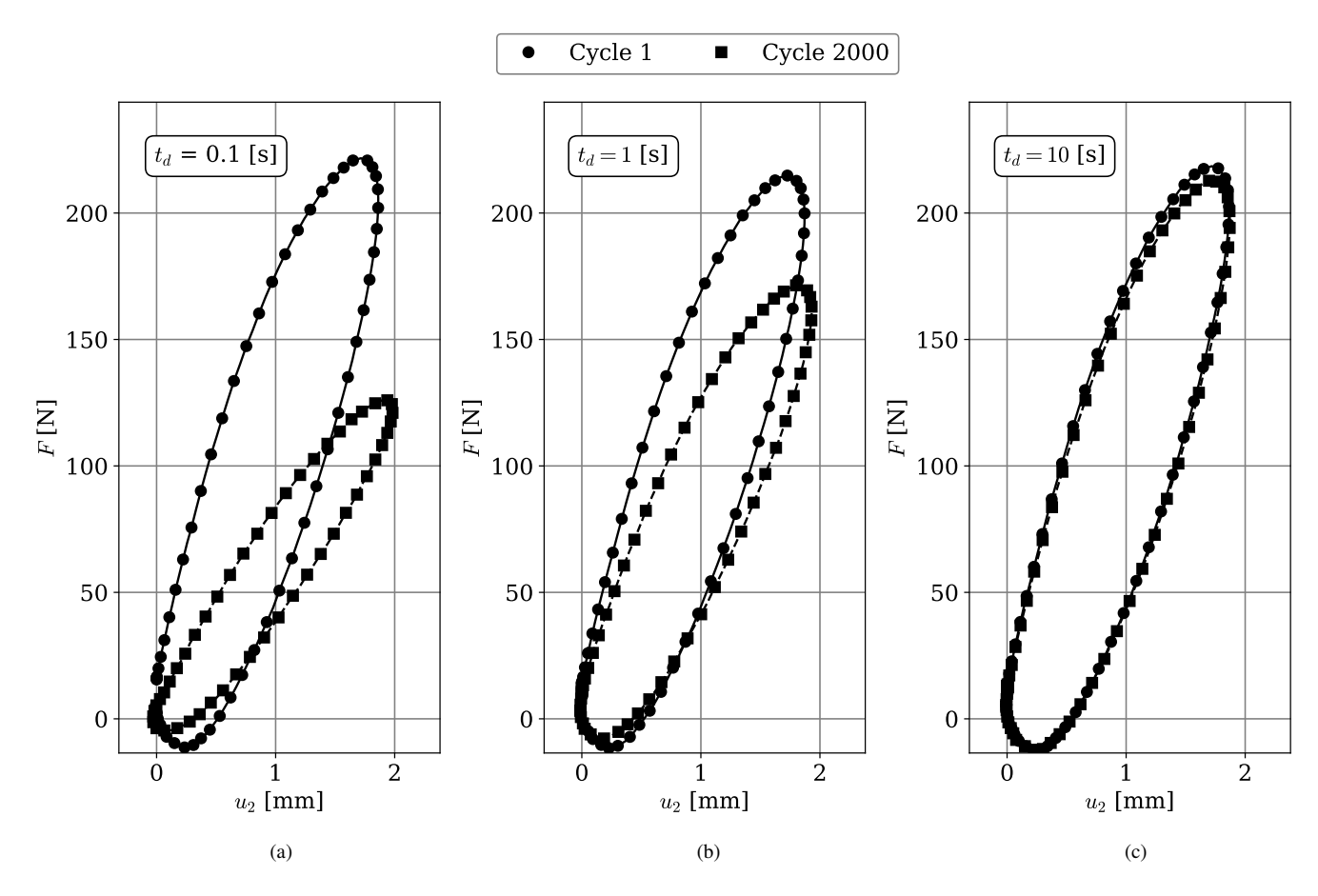


Figure 8. Illustrate load-displacement curves for an uncracked specimen under pulsed loading with a pulse time of  $t_p = 0.1$  s, maximum displacement of  $u_2 = 1.9 - 2$  mm, and dwell times  $t_d \in [0.1, 1, 10]$  s, for the initial (cycle 1) and (cycle 2000) hysteresis loops. Figure (a), (b), and (c) constitutes data from the same sample, which was tested sequentially with a 10-minute recovery period between each test.





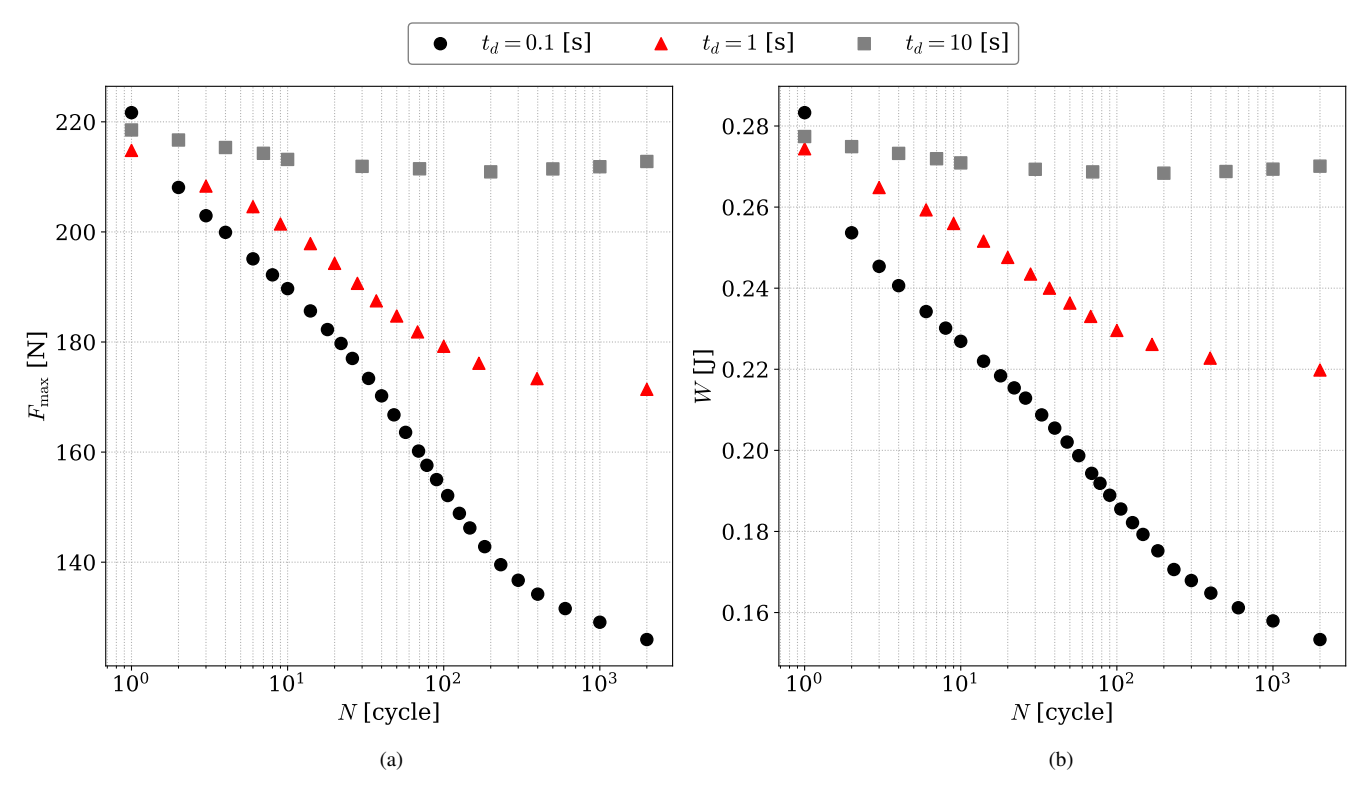


Figure 9. Illustrate the peak load (a) and work under the force deflection curve (b) versus cycle number under pulsed loading with a pulse time of  $t_p = 0.1$  s, maximum displacement of  $u_2 = 1.9 - 2$  mm, and dwell times  $t_d \in [0.1, 1, 10]$  s.





#### 3.2 Fatigue crack growth observations and analysis

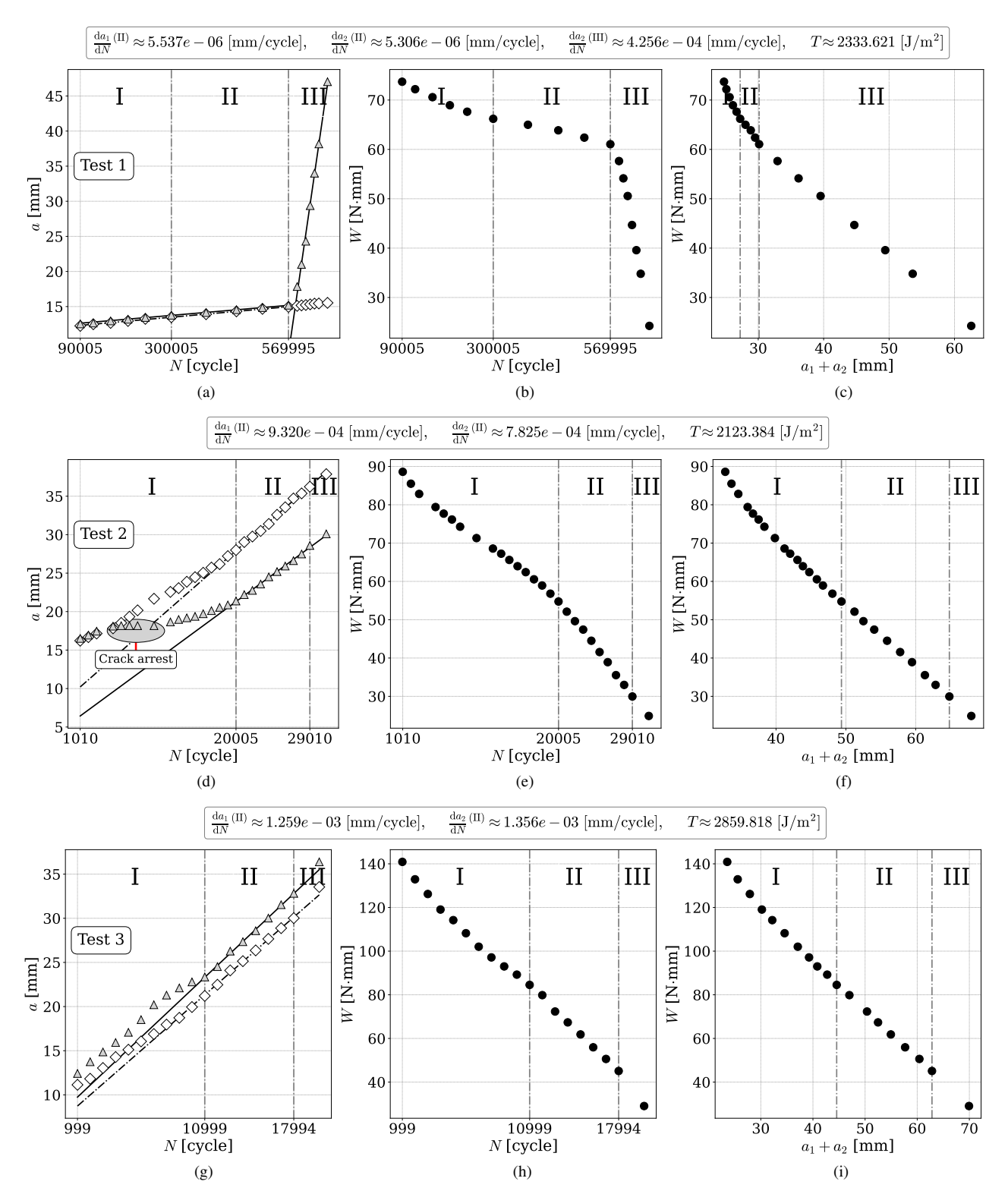
Each test is conducted and analyzed as described in the methods section. Here we describe in detail the observations, features, and analysis of three selected tests, namely tests no. 1, 2, and 3. for which differing crack growth behaviors are observed.

Figure 14 shows plots of the numerical data extracted from these three tests with crack lengths versus cycle number in the first column, loading strain energy versus cycle number in the second column, and loading strain energy versus the sum of crack lengths in the third column. The absolute value of the linear regression  $dW/d(a_1 + a_2)$  is the basis for calculating the tearing energy using Equation 5. For each individual test,  $da_1/dN$ ,  $da_2/dN$  and  $dW/d(a_1 + a_2)$  are evaluated in region II for the same cycle-interval, where the rates are approximately constant. The data are summarized in Table 1.

Table 1. Cycle interval for II in Figure 14, crack growth rate and tearing energy parameters for tests 1, 2, and 3.

Test ID	Cycle Interval [cycles]	$da_1/dN$ [mm/cycle]	$da_2/dN$ [mm/cycle]	$1/b_0 \cdot dW/d(a_1 + a_2) [J/m^2]$
1	300 005–569 995	$5.54 \times 10^{-6}$	$5.31 \times 10^{-6}$	2334
2	20 005–29 010	$9.32 \times 10^{-4}$	$7.83 \times 10^{-4}$	2123
3	10 999–17 994	$1.26 \times 10^{-3}$	$1.36 \times 10^{-3}$	2860





**Figure 10.** First row is specimen no. 1, second is no. 2 and third is no. 3. a,d,f) crack length versus number of cycles. b,e,h) loading strain versus N and c,f,i) loading strain versus the sum of crack lengths.

https://doi.org/10.5194/wes-2025-247 Preprint. Discussion started: 28 November 2025

© Author(s) 2025. CC BY 4.0 License.



300

305

310



In the typical scenario, the two cracks grow at approximately constant and similar rates. However, for some tests discrepancies are observed, which will be addressed in the following.

For test no. 1, Figure 11, the two cracks grow at a rate of around  $5 \cdot 10^{-6}$  mm per cycle for almost 570,000 cycles. Subsequently, the right crack instantly jumps to a rate of  $4 \cdot 10^{-4}$  mm per cycle, also observed within domain III in Figure 14a. Such an abrupt change in crack growth rate was also seen in another specimen. It may indicate that this test was loaded just below a threshold tearing energy, and that the threshold was exceeded for one crack after 570.000 cycles. This may be caused by a slight misalignment of the grips or uneven gripping along the width of the test specimen. It may also be a consequence of the slight increase in peak displacement as the specimen stiffness decreases due to the growing cracks.

Another feature is observed for test no. 2, Figure 12, where the two cracks initially grow at identical rates until around 5000 cycles when the right crack stops while the left crack continues, highlighted as the crack arrest region in Figure 14d. At around 10,000 cycles the right crack finds its way around what appears to be a tough inhomogeneity, and the crack resumes propagation. It then accelerates until around 20,000 cycles, where it reaches its initial rate and grows at the same rate as the left crack. Looking carefully at the photos it can also be seen that the right crack has followed a path that has been affected by the tough inhomogeneity.

Figure 13 shows images from test no. 3, where both cracks grow at a relatively constant rate of approximately  $1.3 \cdot 10^{-3}$  mm per cycle throughout the experiment. A kink angle appears after 5,397 cycles in the left crack, changing the propagation direction of both cracks. This behavior may originate from a local material inhomogeneity or a slight misalignment in the gripping pressure along the specimen length. The change in propagation direction will modify the local strain and stress fields due to a change in principal orientation relative to the global loading direction. However, the calculated work of loading does not indicate any significant change associated with the kink formation, nor is a deviation observed in the crack growth rate, as seen in Figure 10a and 10b. This indicates that the tearing energy, which governs crack advance, is not significantly affected by changes in direction of crack growth.

These observations indicate that a threshold tearing energy exists below which the fatigue crack growth rate is at the order of nanometers per cycle and above which the rates are in the micrometer per cycle range. This threshold may be somewhere in the interval  $T = 2000 - 2400 \text{ J/m}^2$ . The  $\mathrm{d}a/\mathrm{d}N$  versus tearing energy values for all test in the present campaign are presented in the next subsection.





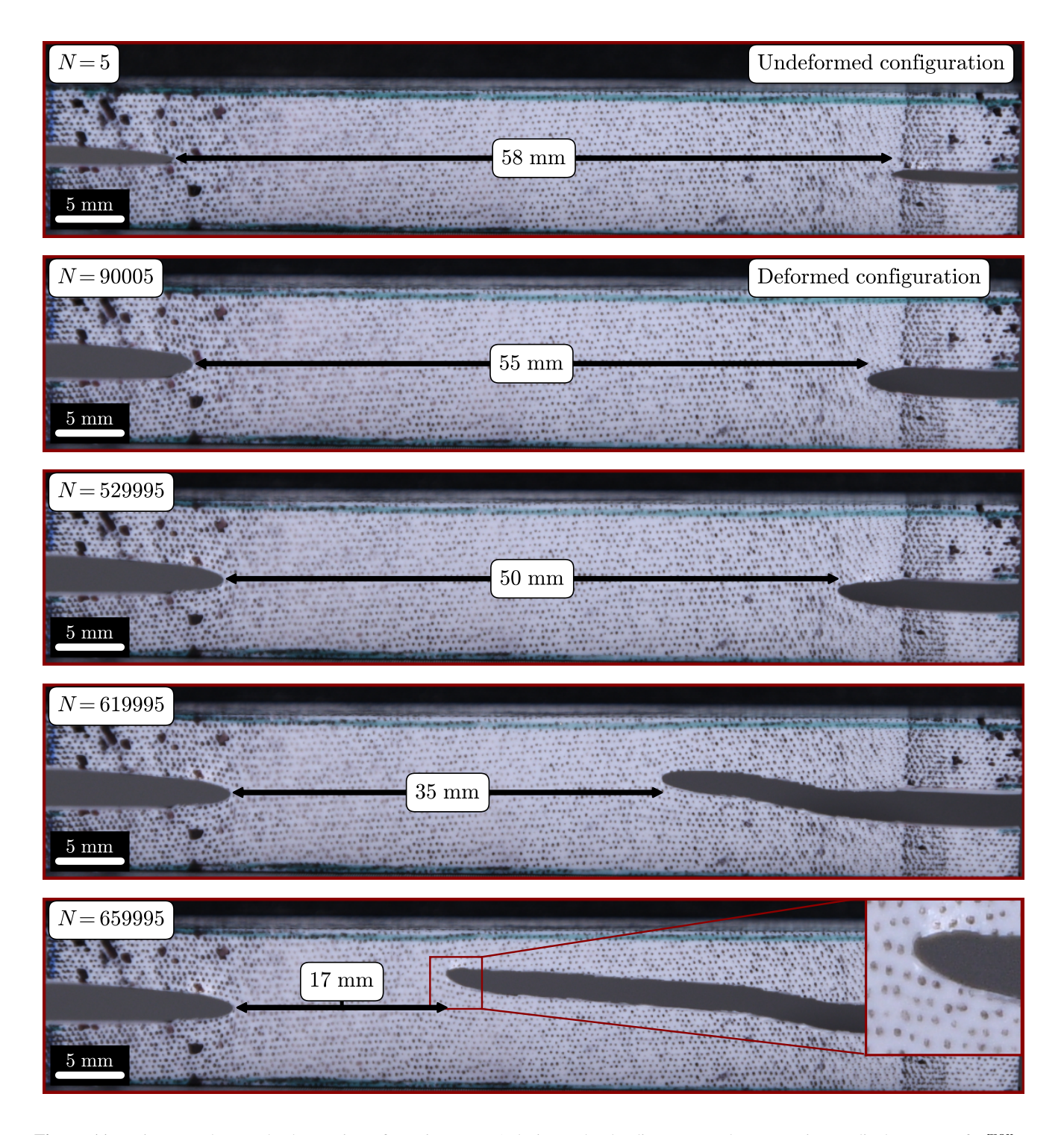


Figure 11. Fatigue crack growth observation of specimen no. 1 during pulse loading, exposed to a maximum displacement of  $u_2^{\text{max}} = 1.53 \, [\text{mm}]$  with a dwell time  $t_d = 0.1 \, [\text{s}]$  and initial crack length  $a_0 = 10 \, [\text{mm}]$ . Numerical data equivalent to the first row in Figure 10.





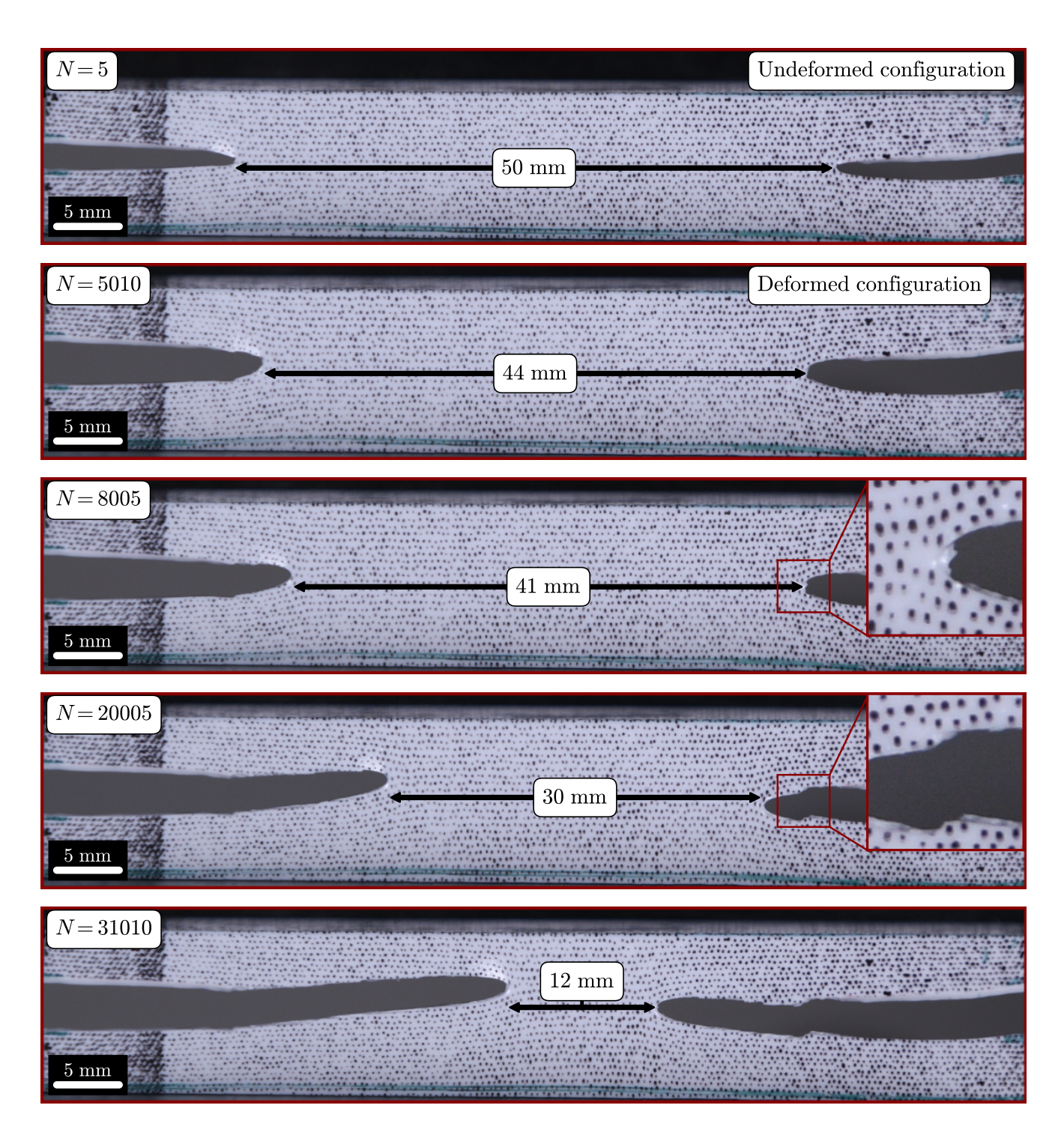


Figure 12. Fatigue crack growth observation of specimen no. 2 during pulse loading, exposed to a maximum displacement of  $u_2^{\text{max}} = 1.76 \, [\text{mm}]$  with a dwell time  $t_d = 0.1 \, [\text{s}]$  and initial crack length  $a_0 = 15 \, [\text{mm}]$ . Numerical data equivalent to the second row in Figure 10.





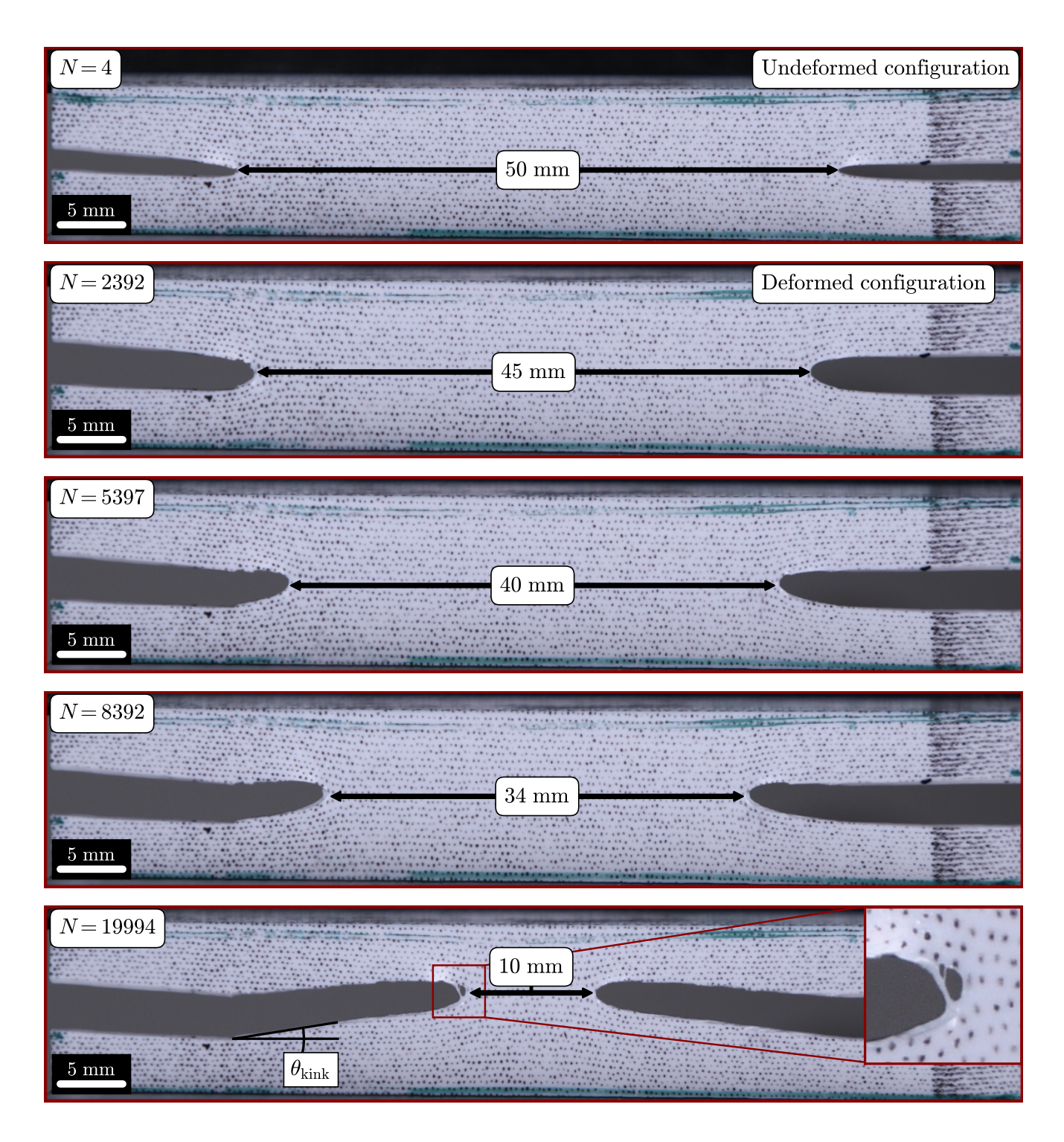


Figure 13. Fatigue crack growth observation of specimen no. 3 during pulse loading, exposed to a maximum displacement of  $u_2^{\text{max}} = 2.07 \, [\text{mm}]$  with a dwell time  $t_d = 0.1 \, [\text{s}]$  and initial crack length  $a_0 = 15 \, [\text{mm}]$ . Numerical data equivalent to the third row in Figure 10.



320

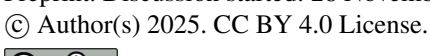


#### 315 3.3 The effect of strain and tearing-energy on crack growth rate

Figure 14a shows crack growth rate da/dN versus peak strain for dwell times of  $t_d \in [0.1,1]$  s.

The strain threshold for crack growth initiation is higher for the experiments conducted with a dwell time of  $t_d=0.1~{\rm s}$  compared to the data points obtained using a dwell time equivalent to  $t_d=1.0~{\rm s}$ . The relative percentage difference is approximately  $\varepsilon_{\rm difference}=27\%$ , as depicted in Figure 14a. Following the trend lines in the growth regimes, it can be stated that for a given input strain, the crack grows faster for  $t_d=1.0~{\rm s}$  than for  $t_d=0.1s$ . Conversely, for a given crack growth rate, the amount of strain required to reach an equivalent growth rate is greater for  $t_d=0.1~{\rm s}$  than for  $t_d=1.0~{\rm seconds}$ . Implying that longer dwell times permit a greater amount of work to be imparted into the system, thereby increasing the energy release rate, which facilitates both crack initiation and accelerated crack growth.

However, it can be observed from Figure 14b that, when inspecting the tearing energy T versus the crack-growth rate,  $\mathrm{d}a/\mathrm{d}N$ , the data collapse across both dwell times,  $t_d \in [0.1, 1.0]$  s, albeit with a slight difference in tearing energy threshold of  $T_{\mathrm{difference}} = 10\%$ . The coincident trend lines indicate that the growth rate over tearing energy is largely independent of dwell time. In contrast (Ghosh et al., 2014) finds that dwell time affects the same correlation in rubber compounds for tires. The preliminary data suggest a tearing energy threshold, below which crack growth is negligible. With the reservation/caveat of limited data points, the threshold is estimated by computing  $T_{\mathrm{thress}} = T_{\mathrm{mean}} \approx 2100 \ \mathrm{J/m}^2$  of the data below  $\mathrm{d}a/\mathrm{d}N < 10^{-4} \ \mathrm{mm/cycle}$  with a  $T_{\mathrm{std}} \approx 200 \ \mathrm{J/m}^2$ .







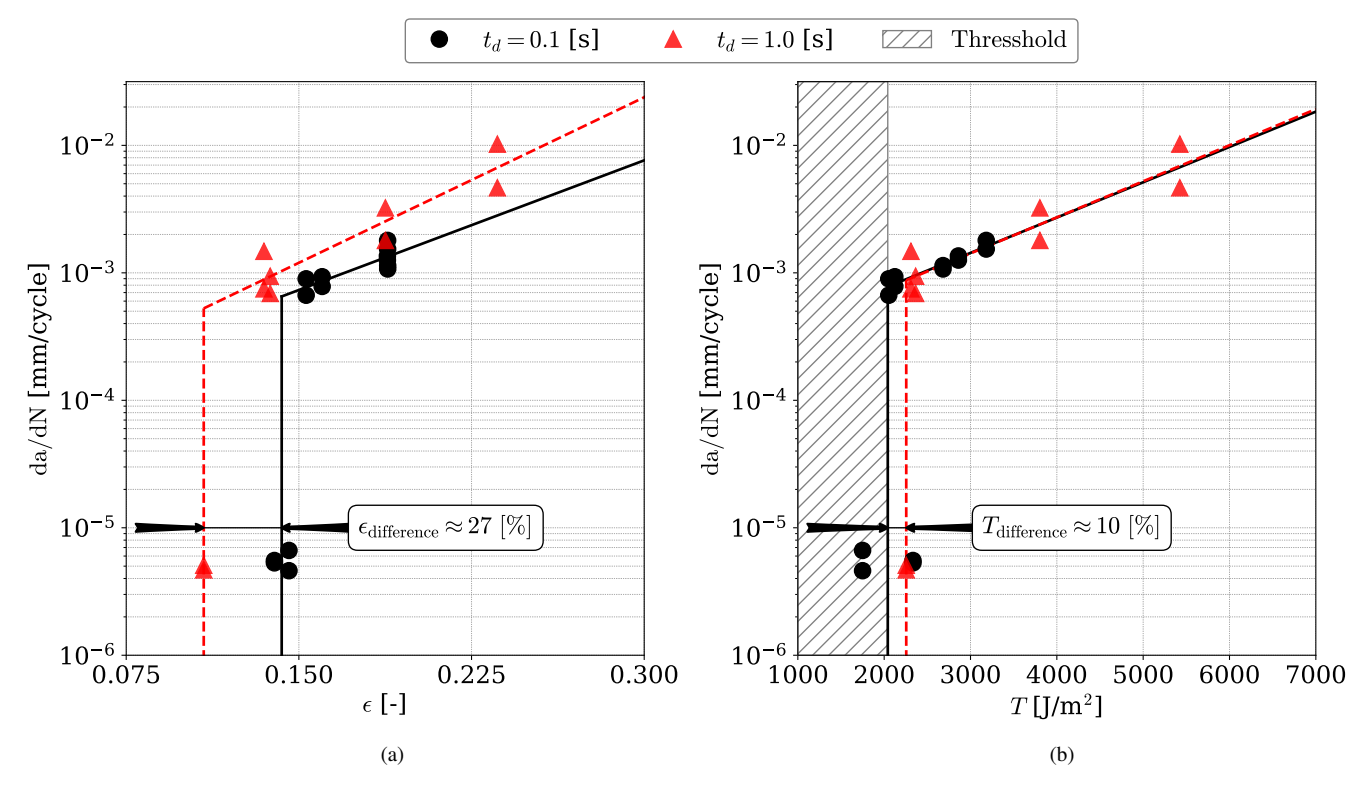


**Figure 14.** crack growth rate versus strain (a) and tearing energy (b) for dwell times of  $t_d \in [0.1, 1]$  s



335

340

345



#### 4 Conclusions, perspectives and future work

The fracture mechanics approach to LEE is probably more appropriate for the assessment of modern LEPs, that fail by local defect induced fatigue cracking, compared to the current stress based linear damage summation approach, that assumes homogeneous properties and continuous progressive damage. This study shows, using fatigue crack growth testing of a polyurethane elastomer sheet, that dwell time influence stress softening and crack growth rate when assessed against peak strain, but not when evaluated against tearing energy. The main messages to convey are as follows.

- 1. The material system exhibits significant time-dependent relaxation during fatigue testing, attributed partly to cyclic stress softening, the Mullins effect. For the short dwell time of 0.1 second, a higher number of cycles is required to reach a stable state with identical subsequent load cycles compared to the longer dwell times of 1 and 10 seconds. Lower dwell times also causes lower peak load and strain energy per cycle when the material has stabilized. The test is considered steady state and material assessment can be conducted when two criteria are fulfilled: 1) the crack growth rates  $da_1/dN$  and  $da_2/dN$  are near similar and constant, and 2) the rate of work over crack propagation  $dW/d(a_1+a_2)$  is constant. A run-in period is required before material assessment can be conducted. Therefore, a strain–energy density function obtained from a monotonic tensile test (as done in conventional methods) is not applicable. Instead, the energy must be evaluated from hysteresis loops recorded for each individual test with its specific test parameters, after the material has stabilized.
- 2. The crack growth rates vary from a few nanometers per cycle below the threshold to some micrometers per cycle above the threshold. In most cases the rates are identical for the two cracks and constant for a the greater part of the test. However, in some tests one of the cracks may stop temporarily or suddenly jump to a higher rate of growth.
- 3. When crack-growth rate was assessed against peak nominal strain, shorter dwell times produced an approximately 27% higher threshold. Conversely, longer dwell times promoted faster growth at a given strain by enabling greater energy input. However, when expressed in terms of tearing energy, the datasets for dwell times between 0.1 and 1.0 seconds nearly coincide, with only about a 10% difference in tearing energy threshold. This indicates that once a stable energy state and mature crack front are established, growth is governed predominantly by the tearing energy rather than by strain.
  - 4. The data suggest the existence of a tearing energy threshold below which crack growth is negligible. With the caveat of limited data points, this threshold is estimated as approximately 2100 J/m<sup>2</sup> with a standard deviation of about 200 J/m<sup>2</sup>.

https://doi.org/10.5194/wes-2025-247 Preprint. Discussion started: 28 November 2025

© Author(s) 2025. CC BY 4.0 License.



365

370



A key finding is the threshold tearing energy below which the fatigue crack growth is negligible. This behavior is particularly valuable for several emerging applications.

- 1. A future parametric model should reflect the role of the governing parameters and properties determining impact fatigue crack growth thresholds for impact on a layered visco-elastic LEP structure. This would imply a dynamic fracture mechanics model that incorporates visco-elastic properties, layered structures, delaminations and cracks of different lengths and orientations.
  - This model should be used to specify target properties when formulating new solutions and to facilitate specification for LEP materials in design guidelines and recommended practices for wind turbine blades.
  - 2. Fracture mechanics in design of LEP materials and systems will provide a mechanistic basis for evaluating LEP systems prior to conventional rain erosion testing and account for basic material properties. By quantifying crack driving forces, energy dissipation mechanisms and crack growth thresholds, it becomes possible to optimize LEP materials and designs for resistance to crack initiation and propagation. This includes tailoring visco-elastic and fracture mechanics properties, interfaces and layer thicknesses to eliminate fatigue cracking and delamination under cyclic impact loading.
  - 3. Erosion safe operation (Bech et al, 2018) is a mitigating strategy, that prevents or delays leading edge erosion. Here the tearing energy threshold for fatigue crack growth could be used as a curtailment criterion in the sense that rotor speed should be kept below a fatigue crack growth propagation threshold which is a function of LEP properties and meteorological conditions like drop size, liquid water content and type of precipitation.
- Fracture mechanics thus offers a potential paradigm shift in handling leading edge erosion of wind turbine blades, and the topic will be pursued and developed in future research. The effect of ultra high strain rates, characteristic for impact, on fatigue crack growth must be explored. Possibly low temperatures could be used to mimic high strain rates as it is common practice for viscoelastic properties using the principle of time-temperature superposition. Rain erosion tests with applied controlled defects should be conducted to establish empirical correlations between fracture mechanics properties and crack growth in rain erosion testing.





# Appendix A

Table A1. General nomenclature

Parameters	Notation	Value	Units
Initial width	$l_0$	80	[mm]
Initial height	$h_0$	10	[mm]
Initial thickness	$b_0$	0.75	[mm]
Crack length	$a_1, a_2$	15 or 10	[mm]
Change in crack length	$\Delta a_1, \Delta a_2$		[mm]
Plane strain zone width	$L_C$		[mm]
Displacement in tension	$u_2$		[mm]
Tensile force	F		[N]
Strain energy density	w		$[J/m^3]$
Strain energy	W		[J]
Tearing energy	T		$[N/m], [J/m^2]$
Dwell time	$t_d$		[s]
Pulse time	$t_p$		[s]
Grip inner radius	$r_i$		[mm]
Grip outer radius	$r_o$		[mm]
Specific impact frequency	$f_i$		[1/s]
Droplet diameter	d		[m]
Droplet impact velocity	$V_{\mathrm{impact}}$		[m/s]
Droplet terminal velocity	$V_{ m droplet}$		[m/s]
Rainfall rate	İ		[m/s]
Liquid volume concentration	Ψ		[-]
Rotations whirling arm RET	Ω		[RPM]
Flow rate	Q		[L/h]
Time between impacts	$\Delta t$		[s]



390



**Table A2.** Field rain scenarios from (Bech et al., 2018)

İ [mm/hour]	d [mm]	V <sub>droplet</sub> [m/s]	$V_{ m impact}$ [m/s]	f [1/s]	$\Delta t$ [s]
1	1.0	3.5	100	0.01	84
3	2.0	6	100	0.01	96
10	3.0	7.5	100	0.02	54
30	4.0	8.8	100	0.04	28

**Table A3.** Rain erosion test parameters at accelerated test speeds, from (Bech et al., 2022)

Needle	$\Omega$ [RPM]	Q [L/h]	d [mm]	V <sub>droplet</sub> [m/s]	$V_{ m impact}$ [m/s]	f [1/s]	$\Delta t$ [s]
G20	1193	120	3.5	2.12	149	0.38	2.63
G27	1193	60	2.8	2.07	149	0.24	4.10
G30	1193	85	1.9	2.32	149	0.45	2.20
G27	1193	105	0.79	2.35	149	1.38	0.72

Author contributions. Author J. I. Bech conducted the experiments and literature study of fatigue studies in rubber like materials and was the primary contributor to the analysis method presented in Section 2.1. Authors J. I. Bech and J. E. Simon contributed equally to the conceptualization, methodology, data analysis, and writing of this paper. Both authors have read and approved the final manuscript and share equal authorship.

Competing interests. The authors declare that they have no conflict of interest.

Acknowledgements. Jamie Simon acknowledge the funding by grant no. 2108-00011B from the Innovation Fund Denmark.

EU Horizon grant no. 101058054 TURBO is acknowledged for supporting the development of the test method and the fixture for the plane strain crack growth test.

The authors would like to acknowledge Théo Larue for contributing in the development of the fixture, and Bent F. Sørensen for healthy debates regarding the J-integral and tearing energy. We would also like to acknowledge Charlotte B. Hasager, and Kristine M. Jespersen, for their reviews.

The authors used ChatGPT and Copilot to refine wording and improve readability in parts of the manuscript. All edits were reviewed by the authors, who take full responsibility for the final content.





#### References

405

- Adler, W. F. and Mihora, D. J.: Analysis of polyurethane advanced rotor blade erosion protection system, Kaman Aerospace Corporation, Bloomfield, CT, Appendix E, 1996, available at: https://apps.dtic.mil/sti/pdfs/ADA314355.pdf
- Amirafshari, P., Brennan, A., and Kolios, A.: A fracture mechanics framework for optimising design and inspection of offshore wind turbine support structures against fatigue failure, WES, 6, 677-699, https://doi.org/10.5194/wes-6-677-2021, 2021
  - Amirzadeh, B., Louhghalam, A., Raessi, M., and Tootkaboni, M.: A computational framework for the analysis of rain-induced erosion in wind turbine blades, part II. Elsevier, 163, 44-54. http://dx.doi.org/10.1016/j.jweia.2016.12.007, 2017.
  - Bai, L., Qv, P., and Zheng, J.: biopolymers Colorless, transparent, and healable silicone elastomers by introducing Zn (II)—carboxylate interactions via aza-Michael reaction, J. Mater. Sci, 55, 14045–14057, https://doi.org/10.1007/s10853-020-04997-6, 2020.
  - Bech, J. I., Hasager, C. B., and Bak, C.: Extending the life of wind turbine blade leading edges by reducing the tip speed during extreme precipitation events, WES, 3, 729–748, https://doi.org/10.5194/wes-3-729-2018, 2018.
  - Bech, J. I., Johansen, N. F. J., Madsen, M. B., Hannesdóttir, Á., and Hasager, C. B.: Experimental study on the effect of drop size in rain erosion test and on lifetime prediction of wind turbine blades, Renew. Energy, 197, 776–789,
- 410 https://doi.org/10.1016/j.renene.2022.06.127, 2022.
  - Bowden, F. P. B. and Brunton, J. H.: The deformation of solids by liquid impact at supersonic speeds, Proc. Roy. Soc., 263, 433–450, https://doi.org/10.1098/rspa.1961.0172, 1961.
  - Caboni, M., Schwarz, A. E., Slot, H., and van der Mijle Meijer, H.: Estimating microplastic emissions from offshore wind turbine blades in the Dutch North Sea, WES, 10, 1123–1136, https://doi.org/10.5194/wes-10-1123-2025, 2025.
- Cardwell, B. J. and Yee, A. F.: Rate and temperature effects on the fracture toughness of a rubber-modified epoxy, Polymer, 34, 1695–1701, https://doi.org/10.1016/0032-3861(93)90329-9, 1993.
  - Cortés, E., Sánchez, F., O'Carroll, A., Madramany, B., Hardiman, M., and Young, T. M, On the material characterisation of wind turbine blade coatings: The effect of interphase coating-laminate adhesion on rain erosion performance, Materials, 10, 1146, https://doi.org/10.3390/ma10101146, 2017.
- DNVGL, DNVGL-RP-0171: Testing of rotor blade erosion protection systems,

  https://www.dnv.com/energy/standards-guidelines/dnv-rp-0171-testing-of-rotor-blade-erosion-protection-systems/, 2018.
  - DNVGL, DNVGL-RP-0573: Evaluation of erosion and delamination for leading edge protection systems of rotor blades, https://www.dnv.com/energy/standards-guidelines/dnv-rp-0573-evaluation-of-erosion-and-delamination-for-leading-edge-protection-systems-of-rotor-blades/, 2020.
- Doagou-Rad, S. and Mishnaevsky, L.: Rain erosion of wind turbine blades: computational analysis of parameters controlling the surface degradation, Meccanica, 55, 725–743, https://doi.org/10.1007/s11012-019-01089-x, 2020.
  - Domenech, L., García-Peñas, V., Šakalyte, A., Francis, D. P., Skoglund, E., and Sánchez, F.: Top coating anti-erosion performance analysis in wind turbine blades depending on relative acoustic impedance. Part 2: Material characterization and rain erosion testing evaluation, Coatings, 10, 1–20, https://doi.org/10.3390/COATINGS10080709, 2020.
- Eisenberg, D., Laustsen, S., and Stege, J.: Wind turbine blade coating leading edge rain erosion model: Development and validation, Wind Energy, 21, 1–10, https://doi.org/10.1002/we.2200, 2018.
  - Evans, A. G., Ito, Y. M., and Rosenblatt, M.: Impact damage thresholds in brittle materials impacted by water drops, J. Appl. Phys., 51, 2473–2482, https://doi.org/10.1063/1.328021, 1980.





- Fraisse, A., Bech, J. I., Borum, K. K., Fedorov, V., Johansen, N. F.-J., McGugan, M., Mishnaevsky, L. Jr., and Kusano, Y.: Impact fatigue damage of coated glass fibre reinforced polymer laminate, Renew. Energy, 126, 1102–1112, https://doi.org/10.1016/j.renene.2018.04.043, 2018.
  - Fæster, S., Johansen, N. F.-J., Mishnaevsky, L. Jr., Kusano, Y., Bech, J. I., and Madsen, M. B.: Rain erosion of wind turbine blades and the effect of air bubbles in the coatings, Wind Energy, 24, 1071-1082, https://doi.org/10.1002/we.2617, 2022.
  - Gent, A. N., Lindley, P. B., and Thomas, A. G.: Cut growth and fatigue of rubbers. I. The relationship between cut growth and fatigue, J. Appl. Polym. Sci., 8, 455–466, https://doi.org/10.1002/app.1964.070080129, 1964.
  - Ghosh, P., Stocek, R., Gehde, M., Mukhopadhyay, R., and Krishnakumar, R.: Investigation of fatigue crack growth characteristics of NR/BR blend based tyre tread compounds, Int. J. Fract., 188, 9–21, https://doi.org/10.1007/s10704-014-9941-9, 2014.
  - Harbour, R.J., Fatemi, A., Mars, W.V.: The Effect of a Dwell Period on Fatigue Crack Growth Rates in Filled SBR and NR, Rubber Chem. Technol., 80, 838–853, https://doi.org/10.5254/1.3539420, 2007
- Herring, R., Domenech, L., Renau, J., Šakalytė, A., Ward, C., Dyer, K., and SGánchez, F.: Assessment of a wind turbine blade erosion lifetime prediction model with industrial protection materials and testing methods, Coatings, 11, https://doi.org/10.3390/coatings11070767, 2021.
  - Hoksbergen, N., Akkerman, R., and Baran, I.: The Springer Model for Lifetime Prediction of Wind Turbine Blade Leading Edge Protection Systems: A Review and Sensitivity Study, Materials (Basel), 15, https://doi.org/10.3390/ma15031170, 2022.
- Hu, W., Chen, W., Wang, X., Jiang, Z., Wang, Y., Verma, A.S., Teuwen, J.J.E.: A computational framework for coating fatigue analysis of wind turbine blades due to rain erosion, Renew. Energy. 170, 236–250. https://doi.org/10.1016/j.renene.2021.01.094, 2021.
  - Ji, Y. M., and Han, K. S.: Fracture mechanics approach for failure of adhesive joints in wind turbine blades, Renew. Energy, 65, 23–28. https://doi.org/10.1016/j.renene.2013.07.004, 2014.
- Jespersen, K. M., Eftekhar, M., Frost-Jensen Johansen, N., Bech, J. I., Mishnaevsky, L., and Mikkelsen, L. P.: High rate response of elastomeric coatings for wind turbine blade erosion protection evaluated through impact tests and numerical models, Int. J. Impact Eng., 179, 104643, https://doi.org/10.1016/j.ijimpeng.2023.104643, 2023.
  - Johansen, N. F.-J.: Test Methods for Evaluating Rain Erosion Performance of Wind Turbine Blade Leading Edge Protection Systems, PhD thesis, Technical University of Denmark, 165 pp.,
    - https://orbit.dtu.dk/en/publications/test-methods-for-evaluating-rain-erosion-performance-of-wind-turb, 2020.
- Jones, S. M., Rehfeld, N., Schreiner, C., and Dyer, K.: The development of a novel thin film test method to evaluate the rain erosion resistance of polyaspartate-based leading edge protection coatings, 14, https://doi.org/10.3390/coatings13111849, 2023.
  - Katsivalis, I., Chanteli, A., Finnegan, W., and Young, T. M.: Mechanical and interfacial characterisation of leading-edge protection materials for wind turbine blade applications, Wind Energy, 25, 1758–1774, https://doi.org/10.1002/we.2767, 2022.
- Keegan, M. H., Nash, D. H., and Stack, M. M.: On erosion issues associated with the leading edge of wind turbine blades, J. Phys. D: Appl. Phys., 46, 383001, https://doi.org/10.1088/0022-3727/46/38/383001, 2013.
  - Kinsley, P., Porteous, S., Jones, S., Subramanian, P., Campo, O., and Dyer, K.: Limitations of Standard Rain Erosion Tests for Wind Turbine Leading Edge Protection Evaluation, Wind, 5, 1–20, https://doi.org/10.3390/wind5010003, 2025.
  - Kocjan, T., Nagode, M., Klemenc, J., and Oman, S.: On fatigue crack growth testing and analysis of non-crystallising rubber using planar tension specimen, Polym. Test., 117, 107819, https://doi.org/10.1016/j.polymertesting.2022.107819, 2023.
- 470 Lake, G. J. and Lindley, P. B.: The mechanical fatigue limit for rubber, J. Appl. Polym. Sci., 9, 1233–1251, https://doi.org/10.1002/app.1965.070090405, 1965.





- Maniaci, D., MacDonald, H., Paquette, J., and Clarke, R.: Leading Edge Erosion Classification System, Sandia National Laboratories (SNL), Albuquerque, NM, and Livermore, CA (United States), pp. 52, https://doi.org/10.2172/2432094, 2022.
- Mishnaevsky, L. and Thomsen, K.: Costs of repair of wind turbine blades: Influence of technology aspects, Wind Energy, 23, 2247–2255, https://doi.org/10.1002/we.2552, 2020.
  - Mishnaevsky, L., Fæster, S., Mikkelsen, L. P., Kusano, Y., and Bech, J. I.: Micromechanisms of leading edge erosion of wind turbine blades: X-ray tomography analysis and computational studies, Wind Energy, 23, 547–562. https://doi.org/10.1002/we.2441, 2020.
  - Pugh, K., Nash, J. W. K., Stack, M. M., and Reaburn, G.: Review of analytical techniques for assessing rain drop erosion resistance of materials, 14th Conference on Sustainable Development of Energy, Water and Environment Systems Dubrovnik, Croatia, 1–6 Oct 2019, https://pureportal.strath.ac.uk/en/publications/review-of-analytical-techniques-for-assessing-rain-drop-erosion-r/, 2019.
  - Rice, J. R.: A path independent integral and the approximate analysis of strain concentration by notches and cracks, J. Appl. Mech., 35, 379–388, https://doi.org/10.1115/1.3601206, 1968.
  - Riddle, T. W., Nelson, J. W., and Cairns, D. S.: Effects of defects in composite wind turbine blades-Part 3: A framework for treating defects as uncertainty variables for blade analysis, Wind Energy Sci, 3, 107–120. https://doi.org/10.5194/wes-3-107-2018, 2018.
- 485 Rivlin, R. S. and Thomas, A. G.: Rupture of Rubber. I. Characteristic Energy for Tearing, J. Polym. Sci., 10, 291–318, https://doi.org/10.1002/pol.1953.120100303, 1953.
  - Stadlbauer, F., Koch, T., Planitzer, F., Fidi, W., and Archodoulaki, V. M.: Setup for evaluation of fatigue crack growth in rubber: Pure shear sample geometries tested in tension-compression mode, Polym. Test., 32, 1045–1051, https://doi.org/10.1016/j.polymertesting.2013.06.003, 2013.
- 490 Harwood, J. A. C., Mullins, L., and Payne, A. R.: Stress Softening in Natural Rubber Vulcanizates. Part II. Stress softening in Pure Gum and Filler Loaded Rubbers, J. Polym. Sci., 9, 3011-3021, https://doi-org.proxy.findit.cvt.dk/10.1002/app.1965.070090907, 1965.
  - Ogden, R. W., and Roxburgh, D. G.: A pseudo-elastic model for the Mullins effect in filled rubber, Proc. R. Soc. A, 455, 2861-2877, https://doi.org/10.1098/rspa.1999.0431, 1998
- Fazekas, B., and Goda T. J.: New numerical stress solutions to calibrate hyper-visco-pseudo-elastic material models effectively. M. Design., 194, 108861, https://doi.org/10.1016/j.matdes.2020.108861, 2020.
  - Sundaraman, S., Hu, J., Chen, J., and Chandrashekhara, K.: Temperature dependent fatigue-failure analysis of V-ribbed serpentine belts, Int. J. Fatigue, 31, 1262-1270, http://dx.doi.org/10.1016/j.ijfatigue.2009.01.019, 2009.
  - Verma, A.S., Wu, C.-Y., Díaz, M.A., Teuwen, J.J.E., Analyzing rain erosion using a Pulsating Jet Erosion Tester (PJET): Effect of droplet impact frequencies and dry intervals on incubation times, Wear, 562–563, https://doi.org/10.1016/j.wear.2024.205614, 2025.
- Vimalakanthan, K., van der Mijle Meijer, H., Bakhmet, I., and Schepers, G.: Computational fluid dynamics (CFD) modeling of actual eroded wind turbine blades, WES, 8, 41–69. https://doi.org/10.5194/wes-8-41-2023, 2023.
  - Visbech, J., Göçmen, T., Özçakmak, Ö. S., Meyer Forsting, A., Hannesdóttir, Á., and Réthoré, P. E.: Aerodynamic effects of leading-edge erosion in wind farm flow modeling, WES, 9, 1811–1826. https://doi.org/10.5194/wes-9-1811-2024, 2024.